Different Trends in Antarctic Temperature and Atmospheric CO2 During the Last Glacial

Zheng, Peisong; Pedro, Joel; Jochum, Markus; Rasmussen, Sune Olander; Lai, Zhongping

Geophysical Research Letters

Key Points:
- The Antarctic warming rate during Antarctic Isotope Maxima significantly decreased as the climate cooled toward the glacial maximum
- In contrast, the rate of millennial-scale CO_2 rise is insensitive to the varying background climate
- The Antarctic warming rate and the rate of millennial-scale CO_2 rise were insensitive to whether the stadial contained a Heinrich event

Author Contributions:

Conceptualization: Peisong Zheng, Joel B. Pedro, Zhongping Lai
Formal analysis: Peisong Zheng, Joel B. Pedro, Markus Jochum, Sune O. Rasmussen
Funding acquisition: Joel B. Pedro, Sune O. Rasmussen, Zhongping Lai
Writing – original draft: Peisong Zheng, Joel B. Pedro
Writing – review & editing: Peisong Zheng, Joel B. Pedro, Markus Jochum, Sune O. Rasmussen, Zhongping Lai

Different Trends in Antarctic Temperature and Atmospheric CO₂ During the Last Glacial

Peisong Zheng[1,2] , **Joel B. Pedro[3,4]**, **Markus Jochum[5]**, **Sune O. Rasmussen[5]** , and **Zhongping Lai[1,6]**

[1]Institute of Marine Sciences, Guangdong Provincial Key Laboratory of Marine Biotechnology, Shantou University, Shantou, China, [2]School of Earth Sciences, China University of Geosciences, Wuhan, China, [3]Australian Antarctic Division, Kingston, Tasmania, Australia, [4]Australian Antarctic Program Partnership, University of Tasmania, Hobart, Tasmania, Australia, [5]Physics of Ice, Climate, and Earth, Niels Bohr Institute, University of Copenhagen, Copenhagen, Denmark, [6]Three Gorges Research Center for Geohazards of MOE, China University of Geosciences, Wuhan, China

Abstract   We analyze the past 67,000 years of climate using Antarctic ice-core records to constrain the mechanisms involved in (a) the "bipolar seesaw" relationship between Greenland and Antarctic surface temperature variations, and (b) mechanisms of millennial-scale atmospheric CO_2 concentration variations. Specifically, we determine for each Greenland Stadial the rate of Antarctic temperature and atmospheric CO_2 rise. We find that Antarctic warming rates significantly decrease as the climate cools during the glacial period, whereas the rate of atmospheric CO_2 rise does not significantly change. Also, we find that the rates of Antarctic warming and atmospheric CO_2 rise are both insensitive to whether a given stadial contains a Heinrich event. These results challenge the view that a single Southern-Ocean-based mechanism dominates the observed glacial variability in Antarctic temperature and atmospheric CO_2. Instead, our results are consistent with an important contribution of low- and mid-latitude processes to millennial-scale atmospheric CO_2 changes.

Plain Language Summary   Glacial climate is characterized by millennial-scale variations in polar temperature and atmospheric CO_2 concentration. The observed similarities between the shape of atmospheric CO_2 and Antarctic temperature records, derived from Antarctic ice cores, have led to a common view that variations in both are dominated by a common Southern Ocean mechanism. However, a systematic comparison of the rates of change of Antarctic temperature and atmospheric CO_2 during these millennia-scale events has not previously been conducted. Furthermore, it is not clearly demonstrated if the rate of change of the Antarctic temperature and atmospheric CO_2 were sensitive to changes in the mean climate state or the occurrence of massive iceberg discharge into the North Atlantic. Here, using ice-core data, we show that the rate of Antarctic warming reduces as the glacial climate cools. In contrast, the rate of atmospheric CO_2 rise is insensitive to glacial cooling. Neither the warming rate nor the rate of atmospheric CO_2 rise are affected by iceberg discharge events. Our result is in contrast with a simple common Southern Ocean control on atmospheric CO_2 and Antarctic temperature and suggests that the millennial-scale atmospheric CO_2 changes include significant contributions from mid-to-low latitudes and processes independent of the background climate.

1. Introduction

During the last glacial period, Greenland ice cores recorded frequent millennial-scale climate changes named Dansgaard-Oeschger (D-O) events (Dansgaard et al., 1993). The events range from a century to many millennia and began with abrupt warming of 5–16°C from a cold phase (a Greenland stadial, GS) to a warm phase (a Greenland interstadial, GI) typically occurring within a few decades (Capron et al., 2021; Huber et al., 2006; Kindler et al., 2014). The Antarctic Isotope Maxima (AIM) are millennial-scale temperature changes with amplitude of 1–3°C identified in Antarctic ice cores (EPICA community members, 2006). After synchronizing Antarctic records to the Greenland ice-core records using records of globally well-mixed atmospheric CH_4, a bipolar seesaw (BPS) pattern is observed between AIM and D-O events (Blunier et al., 1998; EPICA community members, 2006; WAIS Divide Project Members, 2015): the GS coincides with the gradual warming phase of the AIM and the GI coincides with AIM cooling phase (Figure 1) with Antarctica trend changes lagging Greenland transitions by about a century (Svensson et al., 2020; WAIS Divide
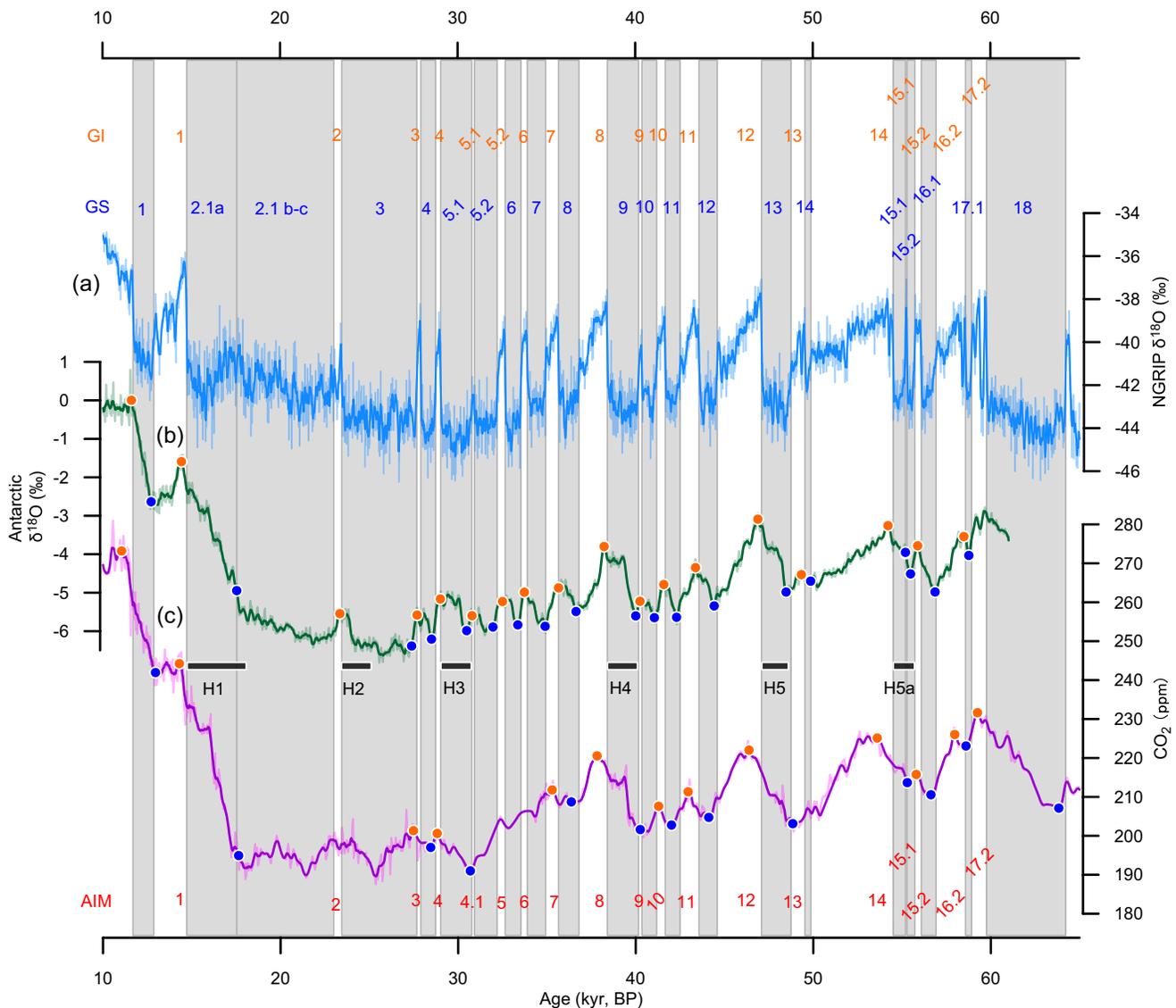
Figure 1. Millennial-scale climate events and atmospheric CO_2 variations for the period 65 to 10 kyr BP. (a) Oxygen isotope ($\delta^{18}O$) data from the North Greenland Ice Core Project (NGRIP) ice core as a qualitative proxy for Greenland temperature (NorthGRIP Project Members, 2004; Svensson et al., 2008). (b) Antarctic five-core averaged $\delta^{18}O$ record (Buizert et al., 2018). (c) West Antarctic Ice Sheet Divide ice-core (WDC) CO_2 record (Bauska et al., 2021; Marcott et al., 2014). The orange and blue dots in (b and c) show the identified Antarctic Isotope Maxima (AIM) and CO_2 maxima and minima, respectively (see text for definitions). (b and c) are on the WD2014 timescale, (a) has been transferred to the WD2014 timescale to match (b and c). The gray vertical shading shows the time spans of the Greenland stadials. Stadials and interstadials are numbered following Rasmussen et al. (2014), the timing of Greenland climate transitions is from Buizert et al. (2015) and WAIS Divide Project Members (2015). The approximate time span of the Heinrich (H) events are marked by the horizontal black bars (Seierstad et al., 2014). The AIM number is following EPICA community members (2006) and extended to AIM17.2.

Project Members, 2015). According to the bipolar ocean seesaw hypothesis (Stocker & Johnsen, 2003), the BPS pattern results from changes in northward heat transport by the Atlantic Meridional Overturning Circulation (AMOC): GS are associated with a weak AMOC, reduced northward heat transport in the Atlantic and warming in the South Atlantic from which AIM warming in Antarctica follows.

The BPS pattern is most pronounced during the Marine Isotope Stage 3 (MIS 3, here defined as 27.5–59.4 kyr BP, thousand years before 1950 A.D.), and is observed throughout the last glacial period (Capron, Landais, Lemieux, & Schilt, 2010; WAIS Divide Project Members, 2015). This raises the question of how the BPS responds to the evolution of the glacial background climate state, in particular the long-term cooling

and increase in ice volume that accompanies MIS 3 and culminates in the last glacial maximum (Clark et al., 2009).

Previous work, based on the European Project for Ice Coring in Antarctica (EPICA) Dronning Maud Land (EDML) ice core, identified a strong linear relationship ($r^2 = 0.85$) between the duration of GS and the amplitude of corresponding AIM surface temperature rises during MIS 3 (EPICA community members, 2006). The linear relationship suggest that the operation of the BPS is not significantly influenced by the evolution of the climate state during the glacial. However, only eleven of the sixteen MIS 3 AIM were considered in the analysis and no significance test was provided. In a later study, when placing EDML oxygen isotope ($\delta^{18}O$) data on a common timescale with the Greenland records (Capron, Landais, Lemieux, & Schilt, 2010), Capron, Landais, Chappellaz, et al. (2010) found that the rate of AIM warming was generally higher in MIS 5 (70.3–130 kyr BP) and low in MIS 2 (17.4–27.5 kyr BP), and that the linear relationship between AIM amplitude and GS duration breaks down for the longest events. The high MIS 5 warming rates indicate that the BPS could be sensitive to the background climate change between different marine isotope stages.

Here we extend these discussions focusing on MIS 3 specifically, as it is characterized by gradual background cooling and frequent BPS events, making it ideal for systematically testing the sensitivity of the BPS to the background climate state.

Furthermore, we test whether the rate of AIM warming is sensitive to the occurrence of Heinrich (H) events, which are characterized by large-scale iceberg discharge into the North Atlantic, suppressing the AMOC with widespread climatic impact (Hemming, 2004; Lynch-Stieglitz, 2016). Previous work disagrees on the impact of H events on Antarctic warming during stadials, with studies proposing that the rate of AIM warming is sensitive (Margari et al., 2010) and others that it is not sensitive (EPICA community members, 2006) to the presence of Heinrich events during stadials.

The apparent similarity between atmospheric CO_2 (hereafter CO_2) concentrations and Antarctic temperature changes in the Antarctic ice-core records (Figure 1) is hypothesized to result from a common cause, such as changes in wind-driven upwelling (Anderson et al., 2009; Anderson & Carr, 2010; Menviel et al., 2018; Toggweiler et al., 2006) or changes in the formation of Antarctic Bottom Water (AABW, Menviel et al, 2015). In both cases, the release of CO_2 and heat involve coupled Southern Ocean processes: increased ventilation of relatively warm and carbon-rich sub-surface waters in the Southern Ocean (Bauska et al., 2018; Gottschalk et al., 2019; Jaccard et al., 2016; Skinner et al., 2020); and/or increased poleward heat transport accompanying the AABW formation and CO_2 ventilation (Menviel et al., 2015).

However, the assumption that millennial-scale CO_2 and Antarctic temperature changes are dominated by common Southern Ocean process is questionable. For example, recent Earth System Model experiments suggest a significant contribution from tropical processes to the millennial-scale CO_2 changes (Nielsen et al., 2019). One way to test this problem is to consider differences between millennial-scale CO_2 and Antarctic temperature changes; two major differences have previously been suggested: (a) CO_2 rises during Heinrich stadials (HS, stadials containing a H event, Barker et al. (2009)) are thought to be of larger amplitude than during non-Heinrich stadials (nHS) (Ahn & Brook, 2014; Bauska et al., 2021); (b) CO_2 maxima of some GS visibly lag the peak of the corresponding AIM events; that is, CO_2 keeps rising after the GI onset and Antarctic cooling have commenced (Figure 1; Bauska et al., 2021; Bereiter et al., 2012). The first difference has been proposed to be caused by a sluggish Southern Ocean response during short GS (Ahn & Brook, 2014; Bauska et al., 2021). Based on the latest high-resolution CO_2 data from WDC, the second difference is suggested to be caused by a superimposed centennial-scale CO_2 rise at the start of the interstadials, probably caused by Northern Hemisphere and tropical processes as suggested by carbon-cycle box-model simulations (Bauska et al., 2021). Thus, whether millennial-scale CO_2 and Antarctic temperature changes are dominated by common Southern Ocean process warrants further investigation.

Here we provide additional analysis by determining the rate of millennial-scale CO_2 rise in the Antarctic ice-core CO_2 data. Using the same statistical tests that are applied to AIM warming rates, we test whether the rate of millennial-scale CO_2 changes are sensitive to the varying background climate state of MIS 3 and different between nHS and HS. The results are then compared to Antarctic temperature to investigate whether CO_2 and Antarctic temperature have the same sensitivity to background climate change and the occurrence of H events.

2. Methods and Results

2.1. The Sensitivity of AIM Temperature Rise to Mean Climate State

We use the recently published Antarctic five-core averaged $\delta^{18}O$ stack (on the WD2014 timescale, data range: 0–61 kyr BP; Buizert et al., 2018) to determine the individual AIM warming amplitudes (in unit of per mille (‰) $\delta^{18}O$). Then, we define the AIM amplitude divided by the corresponding GS duration as the BPS warming rate. The GS durations are obtained from previous work (Buizert et al., 2015).

To obtain a robust estimate for the BPS warming rate and its uncertainty, a Monte Carlo (MC) method is used: in every iteration, the maxima and minima of each AIM are determined from a randomly perturbed version of the five-core averaged $\delta^{18}O$ record which is smoothed with a 200-yr moving average before calculating the BPS warming rate of each AIM. The randomly perturbed $\delta^{18}O$ record is created by drawing values from a normal distribution centered on the five-core averaged $\delta^{18}O$ record with standard deviation set at 0.12‰ (found as the standard deviation of the residual of the smoothed data relative to the unsmoothed). Considering the 100–200 yr lag of the onsets and ends of AIM events relative to Greenland GS and GI transitions (Svensson et al., 2020; WAIS Divide Project Members, 2015), we conservatively search for the isotope maxima and minima in a 300 yr window starting at the time of the corresponding Greenland climate transition. To reduce data uncertainty, we exclude all stadials shorter than 300 years (19 events remain). For GS-2.1a, we observe that a MIS 3-like AIM warming starts about 18 kyr BP (GS-2.1a to 2.1b boundary), and the BPS rate is therefore only determined using GS-2.1a rather than the entire stadial. After 100,000 iterations, the median AIM warming amplitude (Figure 2a) and BPS warming rate (Figure 2b) for each AIM is used as the output, and the 95% confidence interval (CI) of the MC-generated amplitudes and rates of each AIM is used as the estimate of uncertainty range.

We first study whether the BPS warming rates are sensitive to the background climate change of MIS 3. In contrast to the results of EPICA community members (2006), we do not observe a strong linear correlation between MIS 3 GS duration and AIM warming amplitude (Figure 2a). Instead, our data suggest a lower BPS warming rate during late MIS 3 than during early MIS 3 (Figure 2a). To test if this reduction is systematic, we plot the MIS 3 BPS warming rates against the AIM ages (defined as the onset of the corresponding GS). A clear decline in the warming rate across MIS 3 is observed (with a normalized slope of 0.076 unit per kyr, supporting information, Figure 2b). The significance of the observed slope is evaluated by comparing it with the slopes generated from randomly permuting the BPS warming rate data points (keeping the AIM ages) and re-calculating the resulting slopes 100,000 times. In only 0.04% of cases is the absolute value of the randomly generated slope larger than that obtained from the actual data (Figure 2c), demonstrating the declining trend of BPS warming rate during MIS 3 is significant.

Following EPICA community members (2006), our analysis above assumes that the BPS warming rate is linear. If the AIM warming instead is assumed to rise asymptotically as predicted by the "minimum thermodynamic seesaw model" (Stocker & Johnsen, 2003), our definition of the BPS warming rate could be biased toward lower values for longer GS. To test whether our result holds under the assumption of an asymptotic rather than linear temperature increase during AIM, we fit the warming phase of each AIM using the minimum thermodynamic seesaw model (Stocker & Johnsen, 2003; Figure S1): $\Delta T_S = \Delta T_N \left(e^{-t/\tau} - 1 \right)$, where ΔT_S and ΔT_N are the amplitudes of southern warming and northern cooling, respectively, t is the time since the start of the stadial, and τ is the equilibration timescale of the seesaw system, estimated as 1,120 year (Margari et al., 2010; Stocker & Johnsen, 2003). With τ kept constant, we find the amplitude of the fitted line is significantly lowered throughout MIS 3 (in 95% level, with a normalized slope of 0.061 unit per kyr, supporting information, Figure S2, Table S1). Indicating the BPS is also weakening significantly during MIS 3 under the Stocker and Johnsen (2003) minimum thermodynamic seesaw model.

To test whether the AIM warming rates are different between nHS and HS, we group the BPS warming rates into HS and nHS categories (7 and 12 events respectively, Figure 2d). A Student's t-test shows no significant difference (at 95% significance level) between the two categories. Although H events could prolong the stadial duration (Barker et al., 2015), the AIM warming amplitude is not significantly different between HS and nHS (at 95% significance level). These results suggest that the processes controlling Antarctic warming rate are insensitive to the occurrence of H events.
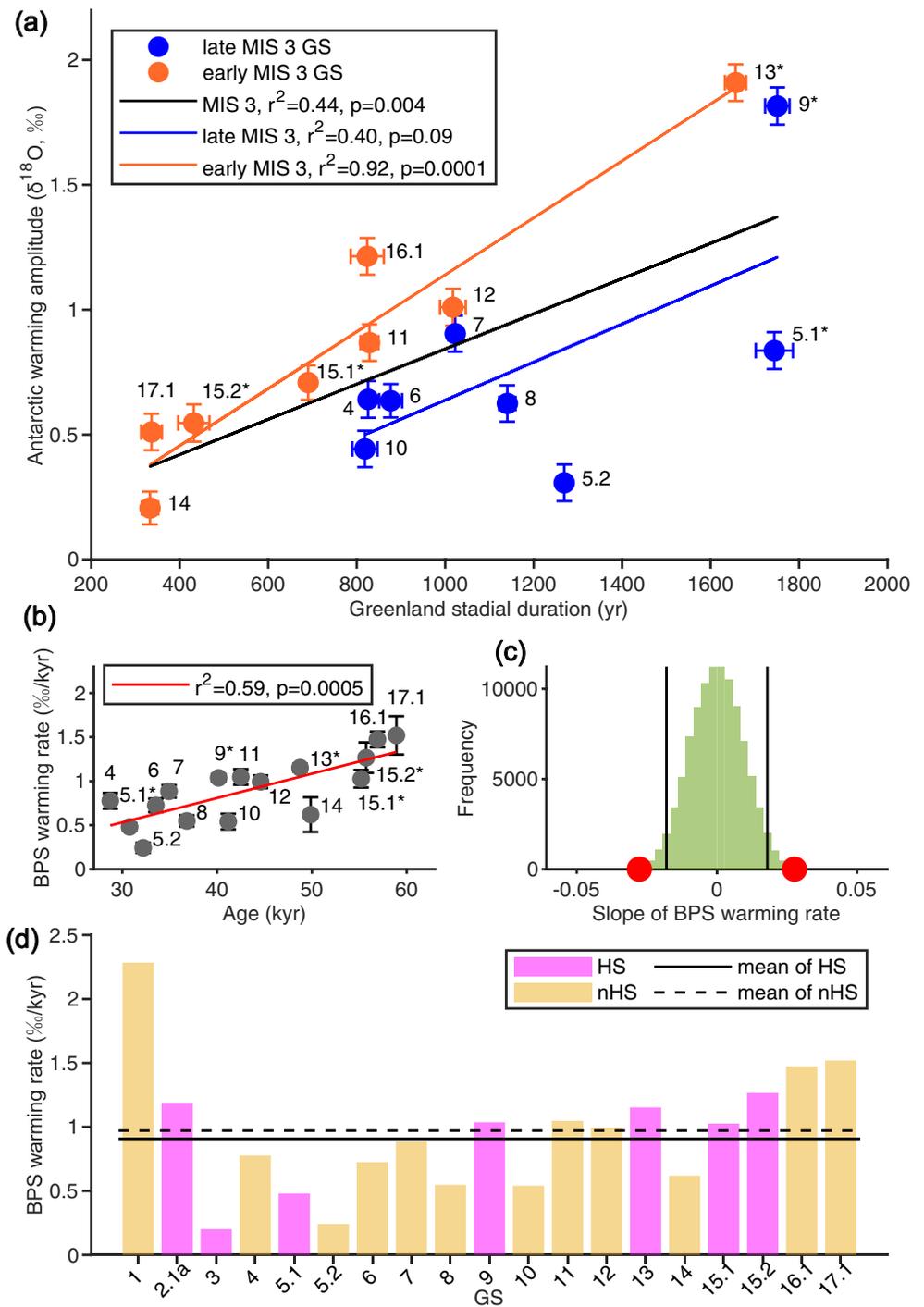
Figure 2. The analysis results for AIM warming. (a) Greenland stadial (GS) duration and Antarctic warming amplitude, the temperature rises are marked by their corresponding GS number. The error bar shows the uncertainty of GS duration (Buizert et al., 2015; WAIS Divide Project Members, 2015) and the 95% confidence interval (CI) of the amplitude. For illustration, MIS 3 events are divided into two equally large groups plotted in different color (early MIS 3 category contains GS-11, 12, 13, 14, 15.1, 15.2, 16.1, and 17.1; late MIS 3 contains GS-4, 5.1, 5.2, 6, 7, 8, 9, and 10). The asterisk denotes HS. (b) Bipolar seesaw (BPS) warming rate plot against the age of the AIM, defined as the initiation of the corresponding GS. The error bar shows the range of 95% CI. (c) Distribution of the slopes of the randomly permuted BPS warming rates, the red dots mark ±1 times the observed slope, the 2.5% and 97.5% fractiles of the randomly generated slope are marked by vertical black lines. (d) Bar chart for Heinrich stadials (HS) and non-Heinrich stadials (nHS) BPS warming rates; note the inclusion of data from MIS 2 (GS-1 and GS-2.1) as well as MIS 3 (GS-3 to GS-17.1).

Our result of a weakening BPS during MIS 3 is robust to replacing GS durations with the duration of the corresponding Antarctic isotope rise (the time between the identified isotope minima and maxima, Table S1). Removing the long-term signal represented by 20,000 yr smoothing of the five-core averaged isotope data, or using unsmoothed five-core average isotope also does not change the conclusions (Table S1, Figure S3). We evaluate the uncertainty of using $\delta^{18}O$ as a proxy for temperature and this uncertainty does not change our conclusion (Supporting Information, Table S1). We also carry out the analysis of the BPS warming rate on the individual ice-core records going into the five-core averaged data set: WDC (WAIS Divide Project Members, 2013, 2015), EDML (EPICA community members, 2006), TALDICE (Landais et al., 2015; Stenni et al., 2010), EDC (EPICA community members, 2004), and Dome Fuji (Kawamura et al., 2007, 2017; Watanabe et al., 2003). Similar results are obtained (Table S1, Figure S3). To test the influence of different timescales, we carry out the same analysis on the $\delta^{18}O$ records on the AICC2012 timescale (EDML, TALDICE, EDC, and Dome Fuji) and find that similar results are obtained (Figure S4, Table S2). Note that as the EDML, EDC and Dome Fuji $\delta^{18}O$ records on the AICC2012 timescale extend through the whole last glacial period, the analysis of HS and nHS BPS warming rate can be extended to GS-25 (110 kyr BP). The results are presented in Figure S4 and Table S2.

2.2. The Sensitivity of Millennial-Scale CO_2 Rise to Mean Climate State

We use the recently published high-resolution WDC CO_2 record (Figure 1, Data range: 8.8–67 kyr BP; average resolution: 88 years; on the WD2014 timescale; Bauska et al., 2021; Marcott et al., 2014) for analysis. A MC method similar to that applied to the warming rate is used to determine the rate of CO_2 rise (supporting information).

Previous research suggests that the CO_2 rise of nHS is close to zero (Ahn & Brook, 2014; Bauska et al., 2021), To account for this, and to remove the effect of short events where the rate of CO_2 increase can be heavily affected by noise, we only include nHS of sufficient amplitude in the subsequent analysis. To determine the threshold of significance, we randomly select two CO_2 data points, then add their corresponding measurement uncertainties in quadrature, and repeat the calculation 100,000 times to estimate the distribution of the uncertainty of the CO_2 amplitudes (Figure S5). A total of thirteen CO_2 rises are identified, six for the HS (GS-2.1a, 5.1, 9, 13, 15.1, 18) and seven for the nHS periods (GS-1, 4, 8, 11, 12, 16.1, 17.1; Figures 1 and 3a).

In contrast to AIM warming rates, the declining trend of MIS 3 CO_2 rates does not stand out clearly (normalized slope of 0.034, Figure 3b), and we do not find evidence for a significant decline in the rate of CO_2 rise across MIS 3 AIM events (two-sided significance: 82.7%, Figure 3c). This is not an artefact caused by the centennial-scale CO_2 rise after the GI onset: when using the CO_2 value sampled at the interstadial onset instead of the CO_2 maxima, also no significant declining trend for CO_2 rates is detected (two-sided significance: 54.9%). The CO_2 trend is also not sensitive to the use of unsmoothed CO_2 data (Figure S6, Table S3) and removing the long-term trend in CO_2 (The long-term trend is represented by 20,000 years smoothing of the CO_2 record) also does not change the conclusion (Figure S6, Table S3). The difference is also not caused by a different number of events considered for CO_2 and Antarctic temperature (see a one-to-one comparison for the same GS in Table S1). Our results are robust to the use of different time scales and CO_2 data set: we perform the same tests using the Bereiter et al. (2015) composite CO_2 record on the AICC2012 timescale instead of the WDC CO_2 record (we use the section originating from Siple Dome, TALDICE and EDML, data range: 22–115 kyr BP). We also test whether a similar pattern is observed in previous glacial periods using the recently recovered high-resolution EDC CO_2 record (on AICC2012 timescale, data range: 330–440 kyr BP, Nehrbass-Ahles et al., 2020), and compare it with the EDC δD record (EPICA community members, 2004). Similar results are obtained (Figures S7 and S8, Table S4).

These results also suggest that our conclusion is not sensitive to the site-dependent bubble enclosure characteristics (or gas diffusion, Bereiter et al., 2015) and depth/age-dependent ice diffusion (Ahn et al., 2008), which both could unevenly smooth the CO_2 record and influence the detection of the long-term trend. We also find that the uncertainty of delta-age (the age difference between gas and ice at the same depth), which could influence the calculated event duration and thus influence the results, does not change our conclusion (Supporting information). The different sensitivity between CO_2 and Antarctic temperature rates is also not sensitive to the statistical method used to detect the trend: we design an alternative test that randomly generates the temporal slope of the CO_2 and Antarctic warming rates from their uncertainty range
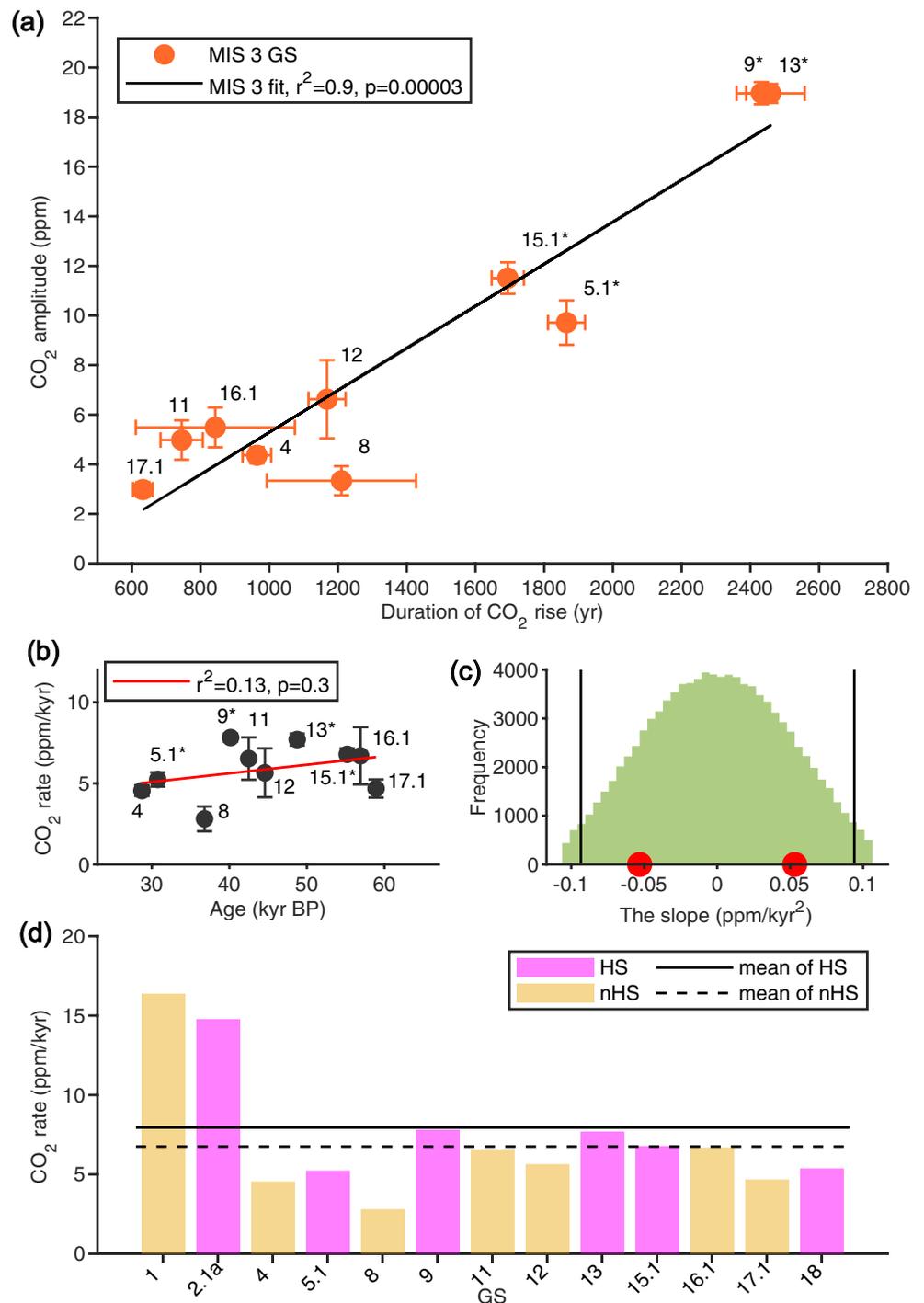
Figure 3. The analysis results for millennial-scale CO_2 rise. (a) CO_2 amplitude versus the duration of CO_2 rises, the error bar shows the 95% confidence interval (CI) of the amplitude and duration. (b) CO_2 rate versus the age of the CO_2 rise, defined as the initiation of the corresponding Greenland stadial. The error bar shows the 95% CI. (c) Comparison between ±1 times the observed slope of the curve in (b) (red dots) with the slopes generated by randomly permuting the CO_2 rate. The 2.5% and 97.5% fractiles of the randomly generated slopes are marked by vertical black lines. (d) Bar chart for Heinrich stadials (HS) and non-Heinrich stadials (nHS) CO_2 rates; note the inclusion of data from MIS 2 (GS-1 and GS-2.1) as well as MIS 3 (GS-4 to GS-18).

(without permuting the rate). The results show a significantly larger temporal slope of the BPS warming rate compared to the temporal slope of the rate of CO_2 rise (in 95% level, supporting information, Figure S9).

We do not find a significant difference between the rate or amplitude of CO_2 rise during HS and nHS (t-test with 95% significance level, Figure 3d, Table S3). The same result is also observed using the composite CO_2 record (Table S4, Bereiter et al., 2012). Note that for the composite CO_2 record, the analysis of HS and nHS CO_2 rates is extended to GS-22 (87 kyr BP, Figure S6, Table S4).

3. Discussion

3.1. Interpreting the Sensitivity of the Bipolar Seesaw to the Mean Climate State

Our statistical analysis suggests that the AIM temperature response during the D-O events is gradually weakened throughout MIS 3. In contrast to previous research that suggested a threshold behavior for the response of the BPS to climate changes (Margari et al., 2010; McManus et al., 1999), our result suggests that the BPS is sensitive to the gradual cooling of the background climate state during MIS 3.

A recent coupled-model investigation of the BPS mechanism (Pedro et al., 2018) suggested that during Greenland stadials, the weakened AMOC drives Antarctic warming through the following chain of events: Reduced northward advection of heat in the Atlantic Ocean results in heat accumulation in the South Atlantic. This heat then spreads east around the globe along the northern edge of the Antarctic Circumpolar Current (ACC). As a result, the temperature gradient across the ACC increases, driving an increase in the cross-ACC heat flux carried by ocean eddies. Temperature anomalies south of the ACC are amplified by the retreat of sea ice and the resulting ice-albedo feedback. Finally, heat from the Southern Ocean sea-ice zone is transported to Antarctica in the atmosphere by storms.

Thus, the declining BPS warming rate could be caused by a lowering in amplitude of the GS AMOC reductions throughout MIS 3, However, this trend is not observed in the reconstructed AMOC strength change during MIS 3 D-O events using $^{231}Pa/^{230}Th$ ratio (Henry et al., 2016), consistent with the Greenland temperature reconstruction, which shows no significant trend in the amplitude of D-O temperature changes during MIS 3 (Kindler et al., 2014).

Cooling of the mean climate state across MIS 3 is shown by Antarctic water isotope records (Buizert et al., 2018), and Southern Hemisphere mid-latitude sea-surface temperature records (Pahnke et al., 2003). We propose that the reduced BPS warming rate results from progressive expansion of Antarctic sea ice over this interval. Expansion of the sea ice expected in a colder climate would lower the efficiency of atmospheric heat transportation from the sea-ice margin to Antarctica, due to the greater distance between Antarctic and the sea-ice-free area. Indeed, Southern Ocean sea-ice expansion at the end of glacial periods is supported by sea-ice proxies, for example, diatom assemblages (Collins et al., 2012; Gersonde et al., 2005; Stuut et al., 2004), the WDC sea-salt Na record (WAIS Divide Project Members, 2015) (Figure S10) and coupled climate model simulations (Ferrari et al., 2014).

3.2. Interpreting the Insensitivity of Millennial-Scale Atmospheric CO_2 Rise to the Mean Climate State

Our results suggest that in contrast to changes in Antarctic temperature, the millennial-scale CO_2 rises are not significantly sensitive to varying background climate during MIS 3. Our results also show that the smaller dependence on CO_2 of background state is observed in earlier glacial periods (Nehrbass-Ahles et al., 2020; Figure S7, Table S4), which suggests it is a robust feature of millennial-scale climate variability during glacial periods. Recent studies propose that increased Southern Ocean deep convection can jointly explain AIM warming and CO_2 trends via the ventilation of heat and CO_2 from the deep ocean (Menviel et al., 2018; Skinner et al., 2020). Carbon reservoir age and deep-water temperature reconstructions from the South Atlantic appear to support this "Southern Ocean hypothesis" during HS-4 (Skinner et al., 2020), but do not quantify the scale of its contribution. Furthermore, although strengthened winds are often invoked as the forcing for increased upwelling, Southern Ocean eddies may nullify the influence of wind changes on upwelling (Munday et al., 2013). Our results on the different sensitivities of AIM temperature trends and CO_2 to the background climate state argue against that a single physical process dominates the millennial-scale

signals in both Antarctic temperature and CO_2 throughout MIS 3. Instead, our results are consistent with a dominant influence of Southern Ocean processes on the AIM temperature evolution (Buizert et al., 2018; Pedro et al., 2018) and an important contribution of low- and mid-latitude processes to CO_2. For example, a reduction of the biological pump (Nielsen et al., 2019) or CO_2 release from terrestrial sources (Bauska et al., 2016; Marcott et al., 2014; Rhodes et al., 2015) would appear consistent with our results. Supporting this argument is the observation that glacial changes in mean climate state at high latitudes are amplified in comparison to their counterparts at low-to-mid latitudes (Annan & Hargreaves, 2013; CLIMAP project members, 1976; MARGO project members, 2009).

Alternatively, our results could be consistent with a common cause by Southern Ocean processes if the ventilation of ocean heat is reduced relative to the CO_2 as MIS 3 progresses and the climate cools, or if heat ventilated by deep convection has less influence on Antarctic temperature due, for example, to expanded Antarctic sea ice (Collins et al., 2012; Gersonde et al., 2005; Stuut et al., 2004). In either case, our observations provide a new target for model studies seeking to replicate the millennial-scale variability of temperature and CO_2 and their sensitivities to climate state and H events.

4. Conclusion

We here studied the sensitivity of millennial-scale Antarctic temperature and atmospheric CO_2 changes to the varying glacial background climate and the presence of Heinrich events. We found markedly different sensitivity of AIM warming rate and CO_2 rate to the gradual change in glacial background climate. We found no significant difference in rate or amplitude response of the millennial-scale Antarctic surface warming or CO_2 rise between stadials with and without Heinrich events, consistent with previous research that suggest that the H events have limited impacts on the dynamics of the BPS (Barker et al., 2015). These results challenge the view that a single Southern-Ocean-based mechanism dominates the observed glacial variability in Antarctic temperature and atmospheric CO_2. Our observations on the rates of change of Antarctic temperature and CO_2 provide a new set of constraints for ongoing studies of the dynamics of millennial-scale climate events and CO_2 changes.

Data Availability Statement

The WDC $\delta^{18}O$ data are available on https://www.nature.com/articles/nature14401#Sec14. The EDML $\delta^{18}O$ data are available on https://www.nature.com/articles/nature05301#Sec2. The EDC $\delta^{18}O$ are available on https://www.ncdc.noaa.gov/paleo-search/study/27950. The TALDICE $\delta^{18}O$ are available on http://www.tal-dice.org/. The Dome Fuji $\delta^{18}O$ data are from multiple researches, and have been compiled in https://www.nature.com/articles/s41586-018-0727-5 (see Buizert et al. (2018) for details). The five-core averaged $\delta^{18}O$ data are available on: https://www.nature.com/articles/s41586-018-0727-5. The WD2014 time scale can be accessed at: https://www.ncdc.noaa.gov/paleo-search/study/20246. The AICC2012 timescale is available on: https://cp.copernicus.org/articles/9/1733/2013/. The WDC CO_2 data can be accessed at: https://www.nature.com/articles/s41561-020-00680-2#Sec15. The composite CO_2 data created by Bereiter et al. (2015) are available on: https://www.ncdc.noaa.gov/paleo/study/17975. The EDC CO_2 data back to 330–440 kyr BP can be accessed at: https://science.sciencemag.org/content/suppl/2020/08/19/369.6506.1000.DC1.

References

Ahn, J., & Brook, E. J. (2014). Siple Dome ice reveals two modes of millennial CO_2 change during the last ice age. *Nature Communications*, *5*(4), 4723. https://doi.org/10.1038/ncomms4723

Ahn, J., Headly, M., Wahlen, M., Brook, E. J., Mayewski, P. A., & Taylor, K. C. (2008). CO_2 diffusion in polar ice: Observations from naturally formed CO_2 spikes in the Siple Dome (Antarctica) ice core. *Journal of Glaciology*, *54*(187), 685–695. https://doi.org/10.3189/002214308786570764

Anderson, R. F., Ali, S., Bradtmiller, L. I., Nielsen, S. H., Fleisher, M. Q., Anderson, B. E., & Burckle, L. H. (2009). Wind-driven upwelling in the Southern Ocean and the deglacial rise in atmospheric CO_2. *Science*, *323*(5920), 1443–1448. https://doi.org/10.1126/science.1167441

Anderson, R. F., & Carr, M.-E. (2010). Paleoclimate. Uncorking the Southern Ocean's vintage CO_2. *Science*, *328*(5982), 1117–1118. https://doi.org/10.1126/science.1190765

Annan, J. D., & Hargreaves, J. C. (2013). A new global reconstruction of temperature changes at the Last Glacial Maximum. *Climate of the Past*, *9*(1), 367–376. https://doi.org/10.5194/cp-9-367-2013

Barker, S., Chen, J., Gong, X., Jonkers, L., Knorr, G., & Thornalley, D. (2015). Icebergs not the trigger for North Atlantic cold events. *Nature*, *520*(7547), 333–336. https://doi.org/10.1038/nature14330

Barker, S., Diz, P., Vautravers, M. J., Pike, J., Knorr, G., Hall, I. R., & Broecker, W. S. (2009). Interhemispheric Atlantic seesaw response during the last deglaciation. *Nature*, *457*(7233), 1097–1102. https://doi.org/10.1038/nature07770

Bauska, T. K., Baggenstos, D., Brook, E. J., Mix, A. C., & Lee, J. E. (2016). Carbon isotopes characterize rapid changes in atmospheric carbon dioxide during the last deglaciation. *Proceedings of the National Academy of Sciences of the United States of America*, *113*(13), 3465–3470. https://doi.org/10.1073/pnas.1513868113

Bauska, T. K., Brook, E. J., Marcott, S. A., Baggenstos, D., Shackleton, S., Severinghaus, J. P., & Petrenko, V. V. (2018). Controls on millennial-scale atmospheric CO_2 variability during the Last Glacial Period. *Geophysical Research Letters*, *45*, 7731–7740. https://doi.org/10.1029/2018gl077881

Bauska, T. K., Marcott, S. A., & Brook, E. J. (2021). Abrupt changes in the global carbon cycle during the last glacial period. *Nature Geoscience*, *14*(2), 91–96. https://doi.org/10.1038/s41561-020-00680-2

Bereiter, B., Eggleston, S., Schmitt, J., Nehrbass Ahles, C., Stocker, T. F., Fischer, H., et al. (2015). Revision of the EPICA Dome C CO_2 record from 800 to 600 kyr before present. *Geophysical Research Letters*, *42*(2), 542–549. https://doi.org/10.1002/2014GL061957

Bereiter, B., Lüthi, D., Siegrist, M., Schüpbach, S., Thomas, F. S., & Fischer, H. (2012). Mode change of millennial CO_2 variability during the last glacial cycle associated with a bipolar marine carbon seesaw. *Proceedings of the National Academy of Sciences of the United States of America*, *109*(25), 9755–9760. https://doi.org/10.1073/pnas.1204069109

Blunier, T., Chappellaz, J., Schwander, J., Dällenbach, A., Stauffer, B., Stocker, T. F., et al. (1998). Asynchrony of Antarctic and Greenland climate change during the last glacial period. *Nature*, *394*(6695), 739–743. https://doi.org/10.1038/29447

Buizert, C., Cuffey, K. M., Severinghaus, J. P., Baggenstos, D., Fudge, T. J., Steig, E. J., et al. (2015). The WAIS Divide deep ice core WD2014 chronology – Part 1: Methane synchronization (68–31 ka BP) and the gas age–ice age difference. *Climate of the Past*, *11*(4), 153–173. https://doi.org/10.5194/cp-11-153-2015

Buizert, C., Sigl, M., Severi, M., Markle, B. R., Wettstein, J. J., McConnell, J. R., et al. (2018). Abrupt ice-age shifts in southern westerly winds and Antarctic climate forced from the north. *Nature*, *563*(7733), 681–685. https://doi.org/10.1038/s41586-018-0727-5

Capron, E., Landais, A., Chappellaz, J., Schilt, A., Buiron, D., Dahl-Jensen, D., et al. (2010). Millennial and sub-millennial scale climatic variations recorded in polar ice cores over the last glacial period. *Climate of the Past*, *6*(3), 345. https://doi.org/10.5194/cp-6-345-2010

Capron, E., Landais, A., Lemieux, B. D., & Schilt, A. (2010). Synchronising EDML and NorthGRIP ice cores using $\delta^{18}O$ of atmospheric oxygen ($\delta^{18}O$atm) and CH_4 measurements over MIS5 (80–123 kyr). *Quaternary Science Reviews*, *29*(1–2), 222–234. https://doi.org/10.1016/j.quascirev.2009.07.014

Capron, E., Rasmussen, S. O., Popp, T. J., Erhardt, T., Fischer, H., Landais, A., et al. (2021). The anatomy of past abrupt warmings recorded in Greenland ice. *Nature Communications*, *12*(1), 2106. https://doi.org/10.1038/s41467-021-22241-w

Clark, P. U., Dyke, A. S., Shakun, J. D., Carlson, A. E., Clark, J., Wohlfarth, B., et al. (2009). The last glacial maximum. *Science*, *325*(5941), 710–714. https://doi.org/10.1126/science.1172873

CLIMAP project members (1976). The Surface of the Ice-Age Earth. *Science*, *191*(4232), 1131–1137. https://doi.org/10.1126/science.191.4232.1131

Collins, L. G., Pike, J., Allen, C. S., & Hodgson, D. A. (2012). High-resolution reconstruction of southwest Atlantic sea-ice and its role in the carbon cycle during marine isotope stages 3 and 2. *Paleoceanography*, *27*(3), PA3217. https://doi.org/10.1029/2011PA002264

Dansgaard, W., Johnsen, S. J., Clausen, H. B., Dahljensen, D., Gundestrup, N. S., Hammer, C. U., et al. (1993). Evidence for general instability of past climate from a 250-kyr ice-core record. *Nature*, *364*(6434), 218–220. https://doi.org/10.1038/364218a0

EPICA community members (2004). Eight glacial cycles from an Antarctic ice core. *Nature*, *429*(6992), 623–628. https://doi.org/10.1038/nature02599

EPICA community members (2006). One-to-one coupling of glacial climate variability in Greenland and Antarctica. *Nature*, *444*(7116), 195–198. https://doi.org/10.1038/nature05301

Ferrari, R., Jansen, M. F., Adkins, J. F., Burke, A., Stewart, A. L., & Thompson, A. F. (2014). Antarctic sea ice control on ocean circulation in present and glacial climates. *Proceedings of the National Academy of Sciences of the United States of America*, *111*(24), 8753–8758. https://doi.org/10.1073/pnas.1323922111

Gersonde, R., Crosta, X., Abelmann, A., & Armand, L. (2005). Sea-surface temperature and sea ice distribution of the Southern Ocean at the EPILOG Last Glacial Maximum—A circum-Antarctic view based on siliceous microfossil records. *Quaternary Science Reviews*, *24*(7), 869–896. https://doi.org/10.1016/j.quascirev.2004.07.015

Gottschalk, J., Battaglia, G., Fischer, H., Frölicher, T. L., Jaccard, S. L., Jeltsch-Thömmes, A., et al. (2019). Mechanisms of millennial-scale atmospheric CO_2 change in numerical model simulations. *Quaternary Science Reviews*, *220*, 30–74. https://doi.org/10.1016/j.quascirev.2019.05.013

Hemming, S. R. (2004). Heinrich events: Massive late Pleistocene detritus layers of the North Atlantic and their global climate imprint. *Reviews of Geophysics*, *42*(1), RG1005. https://doi.org/10.1029/2003RG000128

Henry, L. G., Mcmanus, J. F., Curry, W. B., Roberts, N. L., Piotrowski, A. M., & Keigwin, L. D. (2016). North Atlantic Ocean circulation and abrupt climate change during the last glaciation. *Science*, *353*(6298), 470. https://doi.org/10.1126/science.aaf5529

Huber, C., Leuenberger, M., Spahni, R., Flückiger, J., Schwander, J., Stocker, T. F., et al. (2006). Isotope calibrated Greenland temperature record over Marine Isotope Stage 3 and its relation to CH_4. *Earth & Planetary Science Letters*, *243*(3), 504–519. https://doi.org/10.1016/j.epsl.2006.01.002

Jaccard, S. L., Galbraith, E. D., Martínez-García, A., & Anderson, R. F. (2016). Covariation of deep Southern Ocean oxygenation and atmospheric CO_2 through the last ice age. *Nature*, *530*(7589), 207–210. https://doi.org/10.1038/nature16514

Kawamura, K., Abeouchi, A., Motoyama, H., Ageta, Y., Aoki, S., Azuma, N., et al. (2017). State dependence of climatic instability over the past 720,000 years from Antarctic ice cores and climate modeling. *Science Advances*, *3*(2), e1600446. https://doi.org/10.1126/sciadv.1600446

Kawamura, K., Parrenin, F., Lisiecki, L., Uemura, R., Vimeux, F., Severinghaus, J. P., et al. (2007). Northern Hemisphere forcing of climatic cycles in Antarctica over the past 360,000 years. *Nature*, *448*(7156), 912–916. https://doi.org/10.1038/nature06015

Kindler, P., Guillevic, M., Baumgartner, M. F., Schwander, J., Landais, A., & Leuenberger, M. (2014). Temperature reconstruction from 10 to 120 kyr b2k from the NGRIP ice core. *Climate of the Past*, *10*(2), 887–902. https://doi.org/10.5194/cp-10-887-2014

Landais, A., Masson-Delmotte, V., Stenni, B., Selmo, E., Roche, D. M., Jouzel, J., et al. (2015). A review of the bipolar see–saw from synchronized and high resolution ice core water stable isotope records from Greenland and East Antarctica. *Quaternary Science Reviews*, *114*, 18–32. https://doi.org/10.1016/j.quascirev.2015.01.031

Lynch-Stieglitz, J. (2016). The Atlantic meridional overturning circulation and abrupt climate change. *Annual Review of Marine Science*, *9*(1), 83–104. https://doi.org/10.1146/annurev-marine-010816-060415

Marcott, S. A., Bauska, T. K., Buizert, C., Steig, E. J., Rosen, J. L., Cuffey, K. M., et al. (2014). Centennial-scale changes in the global carbon cycle during the last deglaciation. *Nature*, *514*(7524), 616–619. https://doi.org/10.1038/nature13799

Margari, V., Skinner, L. C., Tzedakis, P. C., Ganopolski, A., Vautravers, M., & Shackleton, N. J. (2010). The nature of millennial-scale climate variability during the past two glacial periods. *Nature Geoscience*, *3*(2), 127–131. https://doi.org/10.1038/ngeo740

MARGO project members (2009). Constraints on the magnitude and patterns of ocean cooling at the Last Glacial Maximum. *Nature Geoscience*, *2*(2), 127–132. https://doi.org/10.1038/ngeo411

McManus, J. F., Oppo, D. W., & Cullen, J. L. (1999). A 0.5-million-year record of millennial-scale climate variability in the North Atlantic. *Science*, *283*(5404), 971–975. https://doi.org/10.1126/science.283.5404.971

Menviel, L., Spence, P., & England, M. H. (2015). Contribution of enhanced Antarctic Bottom Water formation to Antarctic warm events and millennial-scale atmospheric CO_2 increase. *Earth and Planetary Science Letters*, *413*, 37–50. https://doi.org/10.1016/j.epsl.2014.12.050

Menviel, L., Spence, P., Yu, J., Chamberlain, M. A., Matear, R. J., Meissner, K. J., & England, M. H. (2018). Southern Hemisphere westerlies as a driver of the early deglacial atmospheric CO_2 rise. *Nature Communications*, *9*(1), 2503. https://doi.org/10.1038/s41467-018-04876-4

Munday, D. R., Johnson, H. L., & Marshall, D. P. (2013). Eddy saturation of equilibrated circumpolar currents. *Journal of Physical Oceanography*, *43*(3), 507–532. https://doi.org/10.1175/JPO-D-12-095.1

Nehrbass-Ahles, C., Shin, J., Schmitt, J., Bereiter, B., Joos, F., Schilt, A., et al. (2020). Abrupt CO_2 release to the atmosphere under glacial and early interglacial climate conditions. *Science*, *369*(6506), 1000–1005. https://doi.org/10.1126/science.aay8178

Nielsen, S. B., Jochum, M., Pedro, J. B., Eden, C., & Nuterman, R. (2019). Two-Timescale Carbon Cycle Response to an AMOC Collapse. *Paleoceanography and Paleoclimatology*, *34*(4), 511–523. https://doi.org/10.1029/2018PA003481

NorthGRIP Project Members (2004). High-resolution record of Northern Hemisphere climate extending into the last interglacial period. *Nature*, *431*(7005), 147–151. https://doi.org/10.1038/nature02805

Pahnke, K., Zahn, R., Elderfield, H., & Schulz, M. (2003). 340,000-year centennial-scale marine record of southern hemisphere climatic oscillation. *Science*, *301*(5635), 948–952. https://doi.org/10.1126/science.1084451

Pedro, J. B., Jochum, M., Buizert, C., He, F., Barker, S., & Rasmussen, S. O. (2018). Beyond the bipolar seesaw: Toward a process understanding of interhemispheric coupling. *Quaternary Science Reviews*, *192*, 27–46. https://doi.org/10.1016/j.quascirev.2018.05.005

Rasmussen, S. O., Bigler, M., Blockley, S. P., Blunier, T., Buchardt, S. L., Clausen, H. B., et al. (2014). A stratigraphic framework for abrupt climatic changes during the Last Glacial period based on three synchronized Greenland ice-core records: Refining and extending the INTIMATE event stratigraphy. *Quaternary Science Reviews*, *106*, 14–28. https://doi.org/10.1016/j.quascirev.2014.09.007

Rhodes, R. H., Brook, E. J., Chiang, J. C., Blunier, T., Maselli, O. J., Mcconnell, J. R., et al. (2015). Enhanced tropical methane production in response to iceberg discharge in the North Atlantic. *Science*, *348*(6238), 1016–1019. https://doi.org/10.1126/science.1262005

Seierstad, I. K., Abbott, P. M., Bigler, M., Blunier, T., Bourne, A. J., Brook, E., et al. (2014). Consistently dated records from the Greenland GRIP, GISP2 and NGRIP ice cores for the past 104ka reveal regional millennial-scale $\delta^{18}O$ gradients with possible Heinrich event imprint. *Quaternary Science Reviews*, *106*, 29–46. https://doi.org/10.1016/j.quascirev.2014.10.032

Skinner, L., Menviel, L., Broadfield, L., Gottschalk, J., & Greaves, M. (2020). Southern Ocean convection amplified past Antarctic warming and atmospheric CO_2 rise during Heinrich Stadial 4. *Communications Earth & Environment*, *1*(1), 1–8. https://doi.org/10.1038/s43247-020-00024-3

Stenni, B., Masson-Delmotte, V., Selmo, E., Oerter, H., Meyer, H., Röthlisberger, R., et al. (2010). The deuterium excess records of EPICA Dome C and Dronning Maud Land ice cores (East Antarctica). *Quaternary Science Reviews*, *29*(1–2), 146–159. https://doi.org/10.1016/j.quascirev.2009.10.009

Stocker, T. F., & Johnsen, S. J. (2003). A minimum thermodynamic model for the bipolar seesaw. *Paleoceanography*, *18*(4), 1087. https://doi.org/10.1029/2003PA000920

Stuut, J. B. W., Crosta, X., Borg, K. V. D., & Schneider, R. (2004). Relationship between Antarctic sea ice and southwest African climate during the late Quaternary. *Geology*, *32*(10), 909–912. https://doi.org/10.1130/G20709.1

Svensson, A., Andersen, K. K., Bigler, M., Clausen, H. B., Dahljensen, D., Davies, S. M., et al. (2008). A 60 000 year Greenland stratigraphic ice core chronology. *Climate of the Past*, *3*(6), 47–57. https://doi.org/10.5194/cp-4-47-2008

Svensson, A., Dahl-Jensen, D., Steffensen, J. P., Blunier, T., Rasmussen, S. O., Vinther, B. M., et al. (2020). Bipolar volcanic synchronization of abrupt climate change in Greenland and Antarctic ice cores during the last glacial period. *Climate of the Past*, *16*(4), 1565–1580. https://doi.org/10.5194/cp-16-1565-2020

Toggweiler, J. R., Russell, J. L., & Carson, S. R. (2006). Midlatitude westerlies, atmospheric CO_2, and climate change during the ice ages. *Paleoceanography*, *21*(2), PA2005. https://doi.org/10.1029/2005PA001154

WAIS Divide Project Members (2013). Onset of deglacial warming in West Antarctica driven by local orbital forcing. *Nature*, *500*(7463), 440–444. https://doi.org/10.1038/nature12376

WAIS Divide Project Members (2015). Precise interpolar phasing of abrupt climate change during the last ice age. *Nature*, *520*(7549), 661–665. https://doi.org/10.1038/nature14401

Watanabe, O., Jouzel, J., Johnsen, S., Parrenin, F., Shoji, H., & Yoshida, N. (2003). Homogeneous climate variability across East Antarctica over the past three glacial cycles. *Nature*, *422*(6931), 509–512. https://doi.org/10.1038/nature01525

References From the Supporting Information

Barker, S., Knorr, G., Conn, S., Lordsmith, S., Newman, D., & Thornalley, D. (2019). Early interglacial legacy of deglacial climate instability. *Paleoceanography and Paleoclimatology*, *34*(8), 1455–1475. https://doi.org/10.1029/2019PA003661

Fujita, S., Parrenin, F., Severi, M., Motoyama, H., & Wolff, E. W. (2015). Volcanic synchronization of Dome Fuji and Dome C Antarctic deep ice cores over the past 216 kyr. *Climate of the Past*, *11*(10), 1395–1416. https://doi.org/10.5194/cp-11-1395-2015

Jouzel, J., Delaygue, G., Landais, A., Masson-Delmotte, V., Camille, R., & Vimeux, F. (2013). Water isotopes as tools to document oceanic sources of precipitation. *Water Resources Research*, *49*(11), 7469–7486. https://doi.org/10.1002/2013WR013508

Uemura, R., Motoyama, H., Massondelmotte, V., Jouzel, J., Kawamura, K., Gotoazuma, K., et al. (2018). Asynchrony between Antarctic temperature and CO_2 associated with obliquity over the past 720,000 years. *Nature Communications*, *9*(1), 961. https://doi.org/10.1038/s41467-018-03328-3

Veres, D., Bazin, L., Landais, A., Toyé Mahamadou Kele, H., Lemieux-Dudon, B., Parrenin, F., et al. (2013). The Antarctic ice core chronology (AICC2012): An optimized multi-parameter and multi-site dating approach for the last 120 thousand years. *Climate of the Past*, *9*(4), 1733–1748. https://doi.org/10.5194/cp-9-1733-2013